Visualization of Early Intramembranous Ossification by Electron Microscopic and Spectroscopic Imaging

A. LARRY ARSENAULT and F. PETER OTTENSMEYER
Physics Division, Ontario Cancer Institute, Toronto, Ontario Canada M4X 1K9

ABSTRACT We present electron microscopic and electron spectroscopic images of putative nucleation sites and early mineral deposits during intramembranous ossification of the murine perichondrial ring. Electron spectroscopic imaging (ESI) permits the quantitative determination and direct visualization of spatial distribution of atomic elements within specimens at high spatial resolution. In this study ESI was used to determine the elemental distributions of phosphorus, sulfur, and calcium. Nucleation and subsequent mineralization in the perichondrial ring occurred sequentially along the longitudinal axis. Proximal regions of the ring contained a matrix with only a few nucleation sites that are characterized in conventional electron micrographs as small loci of low-density material in which dense particles are located. Elemental maps of these sites that we obtained by ESI reveal a sulfur-containing matrix in which localized concentrations of phosphorus occur. With further maturation the loci became centers for the genesis of numerous dense rods or crystals. These mineral deposits contained increased concentrations of P, S, and Ca, compared with the surrounding matrix. The appearance of S at nucleation sites and its persistence in developing mineral deposits suggests that a sulfur-containing moiety may serve as a locus within the osteoid matrix to attain high local concentrations of Ca and P, which leads to the controlled local formation of calcium phosphates. Calcification of the perichondrial ring has been found to occur in the absence of matrix vesicles, which illustrates that these membrane-bounded organelles are not obligatory sites for nucleation in this matrix.

Attempts to explain the mechanism of mineralization in matrices such as bone, cartilage, dentin, and enamel have led to the rise of several hypotheses each for the most part exclusive of the others. As a result, specific components of both the cell and its extracellular matrix have been implicated in the role of initiating mineralization, or formation of the so-called nucleation site. Several proposed nucleation sites have been reported, for example, mitochondria (28), collagen fibrils (20), interfibrillar structures (35), specific calcification loci (8), and matrix vesicles (6). A large number of authors have accepted matrix vesicles to be the most probable site for nucleation. These vesicles were first reported by Bonucci (9) and later by Anderson (4), who described them as membrane-bounded spheres located in the hypertrophic zone of cartilage growth plate. Matrix vesicles have been subsequently reported in a number of mineralizing matrices (15, 18, 23, 36–38, 42–44). Electron microscopic studies have shown matrix vesicles to contain or to be in close association with the early, solid mineral phase of calcium phosphate and therefore regarded as sites of nucleation (2, 3). However, the mechanism of nucleation in matrix vesicles and the involvement of its limiting membrane in translocating ions are not clearly understood.

Nucleation and mineralization of calcium phosphate compounds are highly regulated by both physical and chemical parameters defined by the organic components of skeletal matrices. An intimate spatial relationship between organic and inorganic components of calcified matrices has been reported by Bonucci (10, 11) using decalcification agents and nonspecific staining reagents such as phosphotungstic acid. These procedures reveal underlying filamentous structures that reflect the crystal morphology of mineral deposits observed in untreated specimens. Thus, these structural components have been called crystal ghosts. The stabilization by cationic dyes and the high sulfur content indicate crystal ghosts to be rich in sulfated glycosaminoglycans (16, 21, 41).

In view of this organic/inorganic relationship within mineral deposits the question therefore re-emerges as to what cellular or matrix component is associated with the initial sites of nucleation. In an attempt to answer this question we

THE JOURNAL OF CELL BIOLOGY · VOLUME 98 MARCH 1984 911–921

have chosen to examine the ossifying perichondrial ring of Lacroix by bright-field electron microscopy and electron spectroscopic imaging (ESI).[1] The latter novel technique permits the direct visualization of atomic elements in entire micrographs with a spatial resolution of 0.3 to 0.5 nm and a minimum detection level as low as 2×10^{-21} g as determined for phosphorus (1, 31). It is well documented that labile ions are extracted from specimens during conventional processing in aqueous media (12, 13, 27). Therefore, to satisfy the need for preservation of both structural and chemical integrities of the bone matrix during the early events of mineralization we have employed both conventionally fixed and cryofixed specimens.

In a previous study, the application of ESI on the mineralizing matrix of epiphyseal growth plates has demonstrated Ca localizations in exact spatial superposition with S in early stages of calcification (7). In that cartilage matrix at later stages the Ca/S relationship is maintained with the addition of Ca/P superposition indicating formation of calcium-phosphorus compounds. The Ca/S overlap suggests that Ca-binding, S-containing moieties (possibly those found in proteoglycans or specific proteins) concentrate Ca ions at specific sites. In this manner the underlying matrix structure may control mineralization.

In this paper the development and mineralization of the perichondrial ring which proceeds sequentially along a longitudinal development gradient was studied. Our examination of this gradient has revealed early sites of nucleation and their pattern of growth. Nucleation sites, spatially close but distinct from both osteoblast extensions and collagen fibrils were characterized by bright field electron microscopy as small, low density aggregates bordered by filamentous extensions. Elemental maps produced by ESI revealed these loci to possess an S-containing matrix and to harbor high local concentrations of phosphorus and scattered, low levels of calcium. With further development these loci became centers for the genesis of mineral deposits that contain dense rod-like structures, the so-called bone crystals. In these developing mineral deposits S persisted in superposition over Ca and P. These results suggest that S-containing moieties may be central in the mechanism of nucleation and provide a means for mediating control over mineralization. Matrix vesicles were not observed within this perichondrial bone matrix.

MATERIALS AND METHODS

Preparation of Specimen

CONVENTIONAL FIXATION: Freshly excised femoral heads from 2-d-old mice (C57BL/6) were immediately placed in 5% glutaraldehyde (pH 7.3) buffered in 0.2 M sodium cacodylate containing 5% sucrose for 1 h at 1°C (over ice). The submersed tissues were cut at once into thin (0.5 mm) slices along the longitudinal axis to facilitate rapid fixation and to ensure planes of section along the mineralization gradient within the developing perichondrial ring of Lacroix. These tissues were rinsed in buffer, postfixed in OsO_4 for 1 h at 1°C, dehydrated in a graded series of ethanol to propylene oxide, and flat embedded in Spurr resin.

CRYOFIXATION: Thin, longitudinally sectioned pieces of fresh femoral heads were plunged into liquid propane cooled by liquid nitrogen. After 10 to 15 s these tissues were transferred to liquid nitrogen contained in a metal beaker fastened to the cooling stage of a Balzers BA360M freeze-etching apparatus (Balzers, Hudson, NH). Specimens were freeze-dried for 14 d at −130°C in a vacuum of 10^{-6} Torr. At this time dry nitrogen gas was introduced into the vacuum chamber raising the pressure to 10 mm of Hg and the temperature was elevated to 20°C. Tissues were transferred to a Speedivac-Pearse tissue-dryer (model 1, Edwards High Vacuum, Oakville, Ontario Canada) and placed under low vacuum in the presence of a 0.5 g crystal of OsO_4 for 1 h. These osmicated specimens were placed in 100% Spurr resin under low vacuum for 3 d, then were brought to atmospheric pressure and polymerized at 65°C for 12 h.

MICROTOMY: A Porter-Blum ultramicrotome Mt-2b (Sorvall, Inc., Norwalk, CT) and a diamond knife were used to cut thin sections exhibiting a silver interference color (60 nm thick) on 4 × distilled water. These sections were examined by bright field electron microscopy. For optimum resolution using ESI extremely thin sections are required. Therefore, only those sections exhibiting a transparent interference color (30–40 nm thick) on 4 × distilled water were immediately placed on 200-mesh grids covered with a fenestrated plastic film that had been stabilized with an evaporated layer of carbon.

Electron Microscopy

For bright-field electron microscopy thin sections were stained with lead citrate followed by 5% aqueous uranyl acetate and examined at 80 kV in a Philips 300 electron microscope. Unstained sections were examined at 80 kV in a Siemens Elmiskop 102 electron microscope equipped with an aberration corrected imaging electron energy loss analyzer (31). The technique of ESI using such a filter has been described elsewhere (31). Briefly, electrons, which have excited the constituent atoms on traversing the specimen, are dispersed by the analyzer into a spectrum of energies in which, after a few low-energy fluctuations, the spectral intensity decreases concurrently with increasing energy loss. Superposed on this falling intensity are step-wise increases in intensity corresponding to electron absorption or ionization edges of specific atomic elements in the specimen. A slit device below the analyzer selects an energy loss just greater than a particular absorption edge which is used to form an image (ESI) that represents the spatial distribution of that element superimposed on the general fine structure of the specimen. Since this image also carries information about the elemental composition of the specimen in a nonspecific manner, a reference ESI that contains only the nonspecific compositional information is taken at an energy loss just below the selected absorption edge. The difference between the two images represents the spatial distribution of the chosen element. Phosphorus, sulfur, and calcium, respectively, were mapped within the ossifying perichondrial ring by bracketing the phosphorus $L_{2,3}$-absorption edge of 132 eV (electron volts) with images taken at 110 and 150 eV, the sulfur edge at 165 eV with ESI's at 150 and 180 eV and the calcium edge at 349 eV with ESI's at 320 and 360 eV.

Net elemental distributions were obtained by digitizing areas of interest on a set of ESIs in 512 × 512 arrays on a Perkin-Elmer microdensitometer (model 1010A; Perkin-Elmer Corp., Norwalk, CT). These images in the form of matrices were aligned, normalized, and subtracted by computer (Digital Equipment Corp., VAX 11/780, Maynard, MA). The elemental maps so obtained were displayed in black and white or color on a video display system (Genisco Computers GCT-300, Costa Mesa, CA) and photographed on a multi-imager (Matrix Instruments, Northvale, NJ).

RESULTS

The ossifying perichondrial ring of Lacroix is a slender collar of bone that circumferentially surrounds the epiphyseal growth plate (Fig. 1); its structural features and cellular origin have been previously described (39). Development and intramembranous ossification of the ring proceed proximally from the growth plate in a sequential fashion along the longitudinal axis. Regions of the perichondrial matrix lying adjacent to the zones of proliferation and hypertrophy were chosen for examination in this study and are shown in Figs. 2 and 3[2], respectively. These areas illustrate the early stages of mineralization prior to the development of heavily calcified areas. The juncture between the growth plate and the ossifying perichondrial matrix is delineated by collagen fibrils separating chondrocytes from rows of aligned, maturing osteoblasts, each interspaced by an extracellular matrix. Distinguishing features of these elongated osteogenic cells are their dense nuclear heterochromatin, well-developed rough endoplasmic

[1] *Abbreviation used in this paper:* ESI, electron spectroscopic imaging.

[2] The specimens shown in Figs. 2–7 were prepared by conventional aqueous means; the specimen in Fig. 8 was prepared by cryofixation methods.

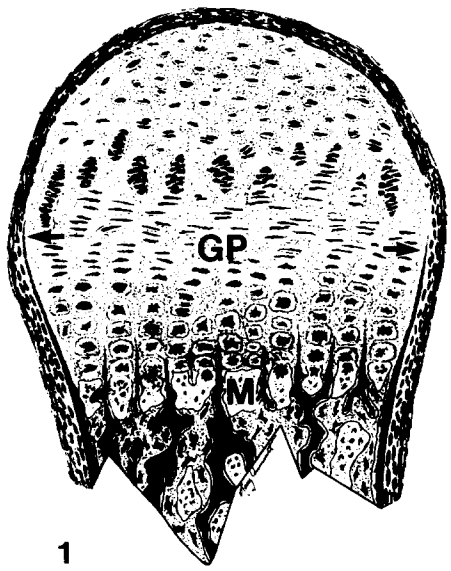

FIGURE 1 A schematic drawn from a light microscopic perspective of the 2 d-old mouse femoral head illustrating the epiphyseal growth plate (*GP*) and the metaphysis (*M*). The perichondrial ring of Lacroix extends along the lateral margin of the growth plate; arrows indicate the sites of initial mineralization chosen for this study.

reticulum, and numerous, extended cell processes. The area of matrix in close proximity to the cartilage growth plate was chosen for study. To compare this matrix with the epiphyseal growth plate matrix a selected area from the zone of hypertrophy is shown at higher magnification as an inset in Fig. 2. This micrograph illustrates a typical matrix vesicle and numerous, densely stained matrix granules. Neither of these distinct cartilage structures were observed in the ossifying perichondrial ring (Figs. 2 and 3).

The bright field image of Fig. 2*a* illustrates two enclosed areas shown at higher magnifications in Figs. 2, *b* and *c*. These areas are spatially separate along the longitudinal axis of the developmental gradient with Fig. 2*b* depicting an earlier stage of development than Fig. 2*c*. The matrix of these images contains osteoblast extensions, collagen fibrils, and an interconnecting network of finely branched filaments. These matrix filaments vary in length, partially due to their orientation within the plane of section; however, their transverse diameter was more consistent at 6–8 nm. Also, within this field are round particles of the same diameter as the filaments. We have interpreted these particles to be filaments that were viewed in cross section and, due to the thickness of the plane of section, appeared more dense than the obliquely orientated filaments. In addition, the distribution of a moderately dense, amorphous material produced a patchy or flocculent appearance to the ground matrix. Within this low density material are denser, rod-shaped structures that vary in length and typically each have a slight curvature. These loci are believed to represent nucleation sites and with further development they acquired characteristics of mineral deposits that included increased density and numerous rod-like structures (compare Fig. 2*b* with 2*c*). Similar mineral deposits shown in Fig. 2*c* have been previously described as calcification loci by Bernard and Pease (8) and crystal islets by Boothroyd (14).

With further development at a level adjacent to the zone of hypertrophy, the perichondrial bone matrix (Fig. 3) was structurally altered by increases in the number of collagen fibrils that occurred both individually and in bundles, osteoblast extensions, and large mineral deposits (bone or calcification nodules [8, 11]). The orientation of the crystal rods within each locus is for the most part random; however, occasionally they were radially arranged. In both cases, for the initial and the more advanced mineral loci, their spatial relationship was close but distinctly separate from collagen fibrils and osteoblast extensions. Morphologically similar mineral deposits have been examined in different mineralizing matrices by x-ray diffraction and x-ray probe microanalysis and are reported to be a solid phase of calcium phosphate in the form of hydroxyapatite (24, 26, 27).

Figs. 4 and 7 are ESIs at 180 eV of an area of unstained perichondrial matrix showing mineral deposits at equivalent stages of development as those in Figs. 2*c* and 3*b*, respectively. Unlike conventional bright-field images, ESI uses only scattered electrons that reveal in high contrast the structural details produced by natural density differences within the section of the specimen. These images appear in reverse contrast to bright-field images, i.e., the denser the specimen structure, the brighter its image. Illustrated in the ESI in Fig. 4*a* are the fine structural details of a nucleation site, early mineral deposits, collagen fibrils, and scattered matrix filaments. The nucleation site and a selected mineral deposit are shown at higher magnifications in Fig. 4, *b* and *c*, respectively. These two loci possess structural features similar to those described for the bright field images (Fig. 2, *b* and *c*). An ESI of a more advanced mineral deposit located near an osteoblast is shown in Fig. 7*a*. These loci (Figs. 4, *b* and *c* and 7*a*) are ESI equivalents to those shown in bright field images in Figs. 2, *b* and *c* and 3*b*, respectively. In ESIs the high densities of these loci appear intimately associated with the surrounding low densities whereas in the bright field images the more densely stained areas are sharply enhanced over the less densely stained material. This demarcation in bright field is due to the preferential masking by heavy metals and to defocused phase effect enhancement. Unstained ESIs are not subject to either of these resolution limiting factors and therefore represent a more correct image of the natural fine structure. Optical laser analysis of the bright field, electron image plates from which the micrographs shown in Figs. 2 and 3 were produced reveals a resolution limitation of ~3 nm due to phase effects.

The elemental distributions of P, S, and Ca of the nucleation site in Fig. 4*b* are shown as individual elemental maps in Fig. 5, *a*, *b*, and *c*, respectively. Sulfur is distributed homogeneously over the entire site whereas P, in addition to having a similar distribution to S, appears highly localized over the punctate, electron-dense areas shown in Fig. 4*b*. The distribution of both P and S superimposes over the osteoblast extensions and collagen fibrils. Calcium appears more homogeneously dispersed throughout the matrix with only a slight aggregation at the nucleation site. This low level of Ca present within this locus may have resulted from dissolution by the aqueous media used during tissue preparation. However, calcium is highly localized within the osteoblast extension (Fig. 5*c*).

Similar to the nucleation locus (Fig. 4*b*), the early mineral deposit shown in Fig. 4*c* is in close proximity to collagen fibrils and osteoblast extensions. Also, the dense core is bordered by filaments that extend into an amphorous, low density material in contact with collagen fibrils and cellular processes. Elemental maps for P, S, and Ca of the early mineral deposit shown in Fig. 4 are displayed in Fig. 6, *a*, *b*, and *c*, respectively.

The levels of these elements in the general ground substance were low; however, they occurred at high concentrations within the locus. The phosphorus and sulfur maps illustrate elemental distribution reflective of the general morphology of the locus and a nearby collagen fibril. The periphery of the locus exhibits P- and S-containing filaments that project into the surrounding ground matrix. In contrast, the Ca distribution is more restricted to the locus core at which site all three elements are in superposition.

Electron spectroscopic analysis of a more advanced mineral deposit reveal a superpositioning of P, S, and Ca as shown in Fig. 7, *b*, *c*, and *d*, respectively. The P and S distributions reflect the internal organization of the rod-like structures within the deposit. Calcium, on the other hand, appears rather sparse. A cryofixed mineral deposit at a similar stage of advancement is shown in Fig. 8*a* with superpositioned maps of P, S, and Ca displayed in Fig. 8, *b*, *c*, and *d*, respectively. In these cryofixed deposits the internal morphology and elemental distributions are more homogeneous compared with the dense, rod-shaped structures of mineral deposits processed by aqueous means (Figs. 3*b* and 7*a*). This structural homogeneity may be due to the increased retention of various ions and macromolecules by cryofixation resulting in an overall increased mass density that masked the otherwise visible structures observed in aqueously processed tissues. The intense localization of Ca within the cryofixed mineral deposit (Fig. 8*d*) ranges from 500 to 800 atoms/nm^2 as compared with 40 to 60 atoms/nm^2 of Ca in the aqueously processed specimen (Fig. 7*d*). Quantification of atomic elements by ESI has been previously described (32).

DISCUSSION

A variety of tissue preparative methods for electron microscopy have been developed each with their own characteristics for the preservation of structural details and associated chemistry. In the study of bone and cartilage, aqueously processed tissues have been coupled with various stains to stabilize anionic proteoglycans (22, 40, 45). Also, in attempts to reduce the possibilities of ion translocation, artifactual precipitations, and mineral phase transformations in these matrices, anhydrous and ultracryomicrotomy techniques have been employed (19, 24–27). These alternate methods have proven extremely useful in the preservation of detection of proteoglycans and for the preservation of labile ions. However, they typically provide poor definition of fine structural details due to stain masking in the case of precipitation procedures for proteoglycans, and thick specimen sections and ice crystal damage in cryosections. To achieve the high spatial resolution capabilities of ESI we have used conventionally prepared and cryofixed tissues embedded in resin. Ultrathin sections (30–40 nm thick) of plastic embedded material can be readily obtained enabling the detection of exquisite structural details and higher spatial resolution of elemental distributions. Conventional tissue processing has the drawback of dissolution of labile ions and this has been aptly demonstrated for bone (12, 13). This is further suggested in the present study by the observed 10–15-fold increase of Ca in cryofixed mineral deposits compared with those processed by aqueous means. Effectively, conventional processing serves to partially demineralize calcified tissues; however spurious translocation and reprecipitation of ions were not evident in the perichondrial bone matrix.

The present study has revealed that mineralization in the perichondrial ring occurs along a well-defined, developmental gradient. Examination of this gradient along the longitudinal axis of the ring enabled the visualization of the transition from a noncalcified to a calcified matrix. The earliest events of this transition were the formation of nucleation sites defined as distinct loci spatially separate but in close proximity to collagen fibrils and osteoblast extensions. These sites possess a heterogeneous fine structure reflecting their origin as localized condensations of extracellular components. The direct ESI visualization of elements at these sites revealed a generalized distribution of S and P, with P also locally concentrated in a punctate fashion. Calcium, although present occurred more homogeneously distributed throughout the matrix. This distribution contrasts with ESI observations in epiphyseal growth plate where S and Ca appear in virtual superposition at early sites of mineralization, while P is highly localized in granules (7). In the perichondrial matrix the superpositioning of P, S, and Ca are attained at slightly later stages of mineral deposit development as was similarly observed in more developed mineral deposits within the growth

FIGURE 2 (*a*) Murine femoral head viewed at the cartilage zone of proliferation showing the perichondrium-cartilage junction. Elongated osteoblasts (*Ob*) exhibit numerous cytoplasmic extensions (arrows) scattered throughout the perichondrial matrix. The enclosed areas that are labeled *b* and *c* represent sequential stages of nucleation located along the longitudinal axis and are shown at a higher magnification in *b* and *c*, respectively. *Ch*, chondrocyte. The *inset* (*a*) is an area of the epiphyseal zone of hypertrophy showing a typical matrix vesicle (*MV*) and intensely stained matrix granules (*MG*). (*b*) Nucleation sites (arrows) consisting of dense, needle-like crystals embedded in a fibrous matrix. *f*, matrix filaments; *Ob*, osteoblast extensions. (*c*) A mineral deposit locus (arrow) located distally with respect to *b* showing an increased electron density and elongated crystal rods. Bars, 2.5 μm (*a*); 0.1 μm (*a*, *inset*); 0.3 μm (*b* and *c*). × 8,000 (*a*); × 83,200 (*inset*); × 75,500 (*b* and *c*).

FIGURE 3 (*a*) The perichondrial matrix adjacent to the cartilage zone of hypertrophy, distal to the view shown in Fig. 2*a*. This matrix contains bundles of collagen fibrils (*cf*), osteoblast extensions (arrows), and numerous mineral deposits (*MD*). *Ob*, osteoblast. Enclosed area is shown at a higher magnification in Fig. 3*b*. (*b*) An area with numerous mineral deposit loci (arrows) showing proximity to collagen fibrils (*cf*) and osteoblast processes (*Ob*). Each locus contains heavily stained rod-shaped structures embedded in a more lucent matrix. Bars, 2 μm (*a*); 0.3 μm (*b*). × 9,000 (*a*); × 75,500 (*b*).

FIGURE 4 (*a*) Electron spectroscopic image at 180 eV of an unstained section of perichondrial matrix at a level just distal to that shown in Fig. 2*a*. This image is in reverse contrast to conventional bright-field images and is not subject to phase effects. A nucleation site (arrow) is located adjacent to a dense osteoblast extension (*Ob*). Along the right margin of the image early mineral deposits (*MD*) are found in close proximity to collagen fibrils (*cf*) and cellular extensions (*Ob*). The nucleation site and an early mineral deposit are shown at higher magnification in *b* and *c*. Bars, 0.4 μm (*a*); × 0.1 μm (*b* and *c*). × 53,000 (*a*); × 212,000 (*b* and *c*).

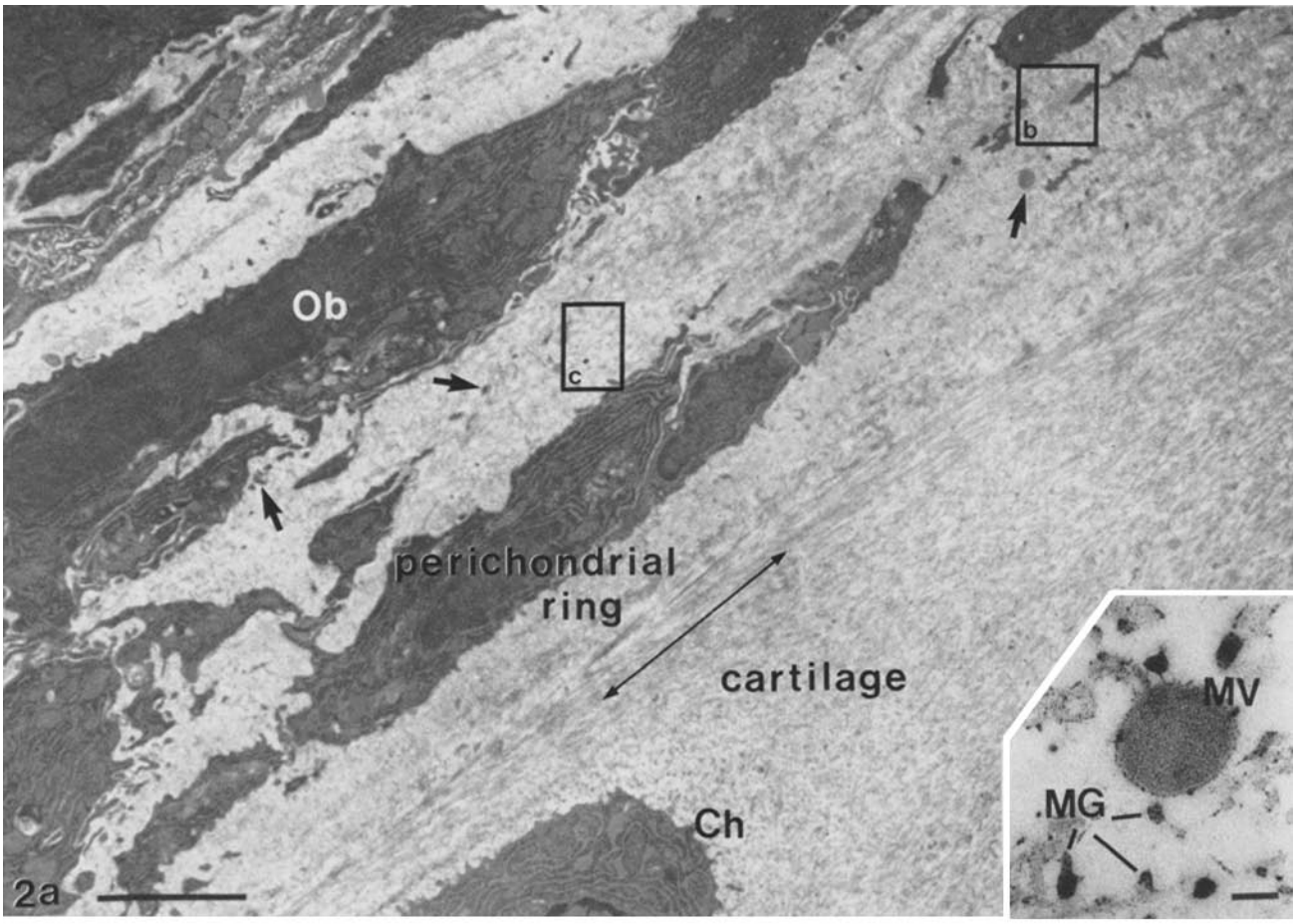
Ob
b
c
perichondrial
ring
cartilage
Ch
MV
MG
2a

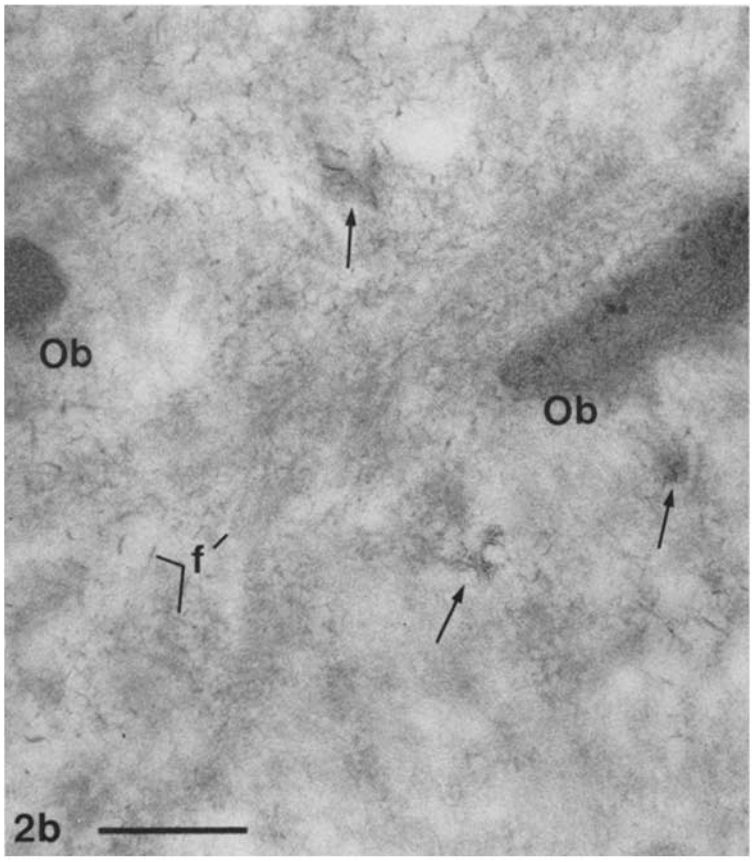
Ob
Ob
f
2b

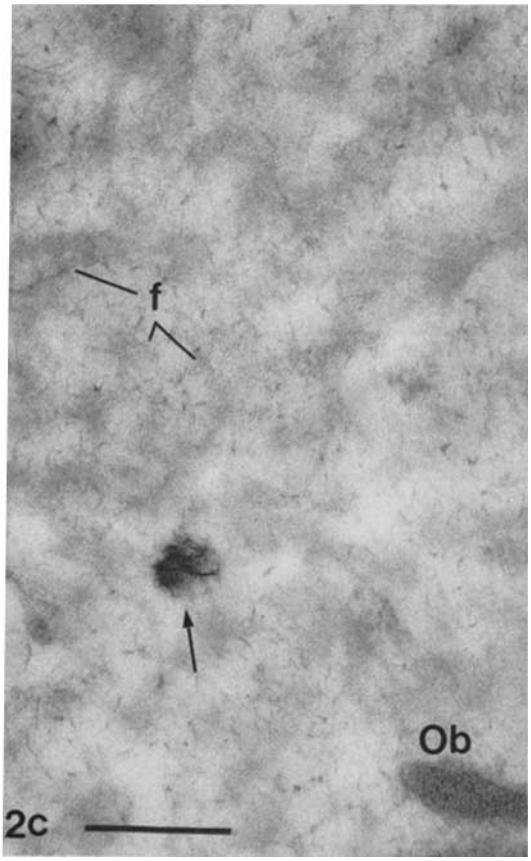
f
Ob
2c

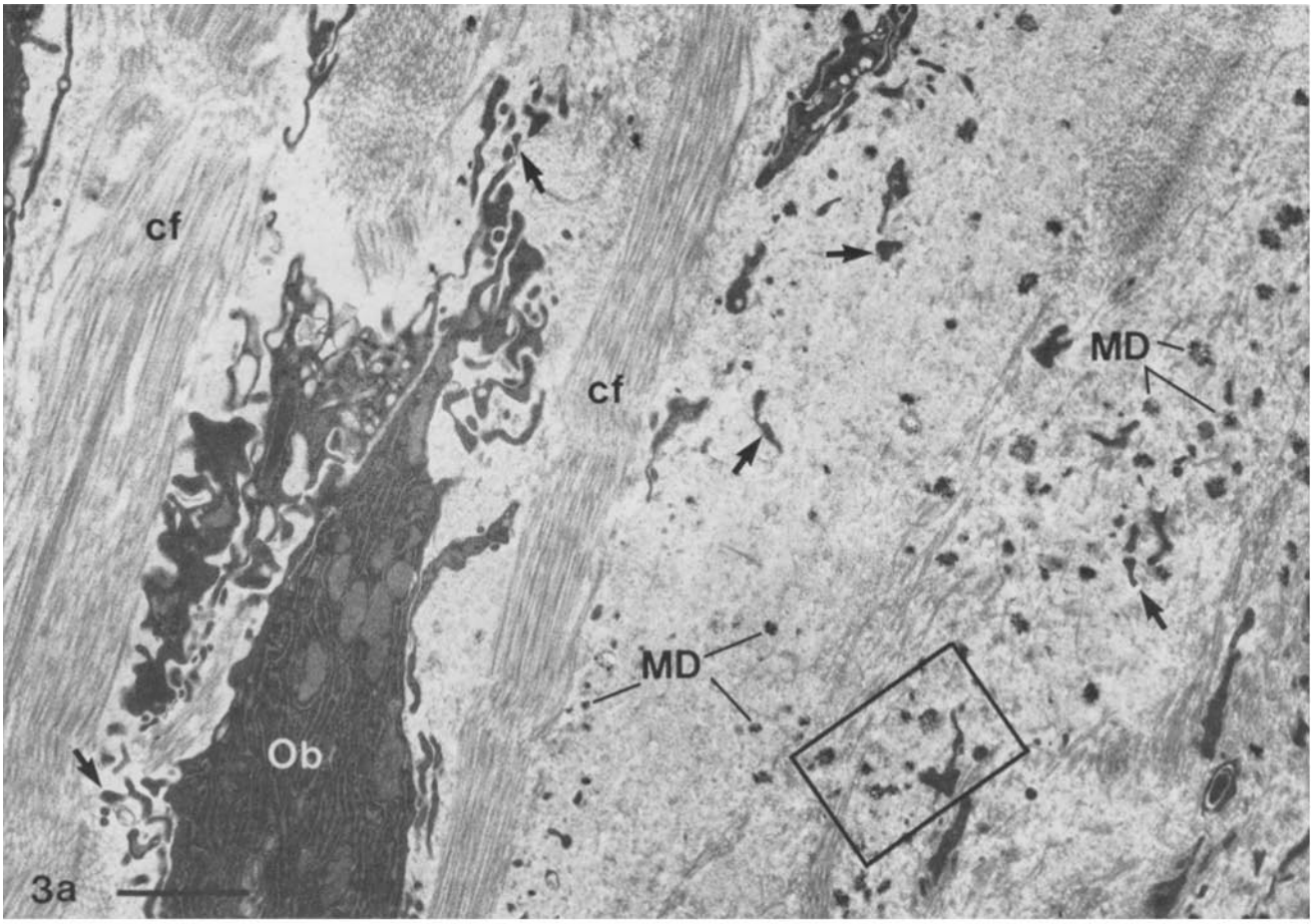
cf
cf
MD
MD
Ob
3a

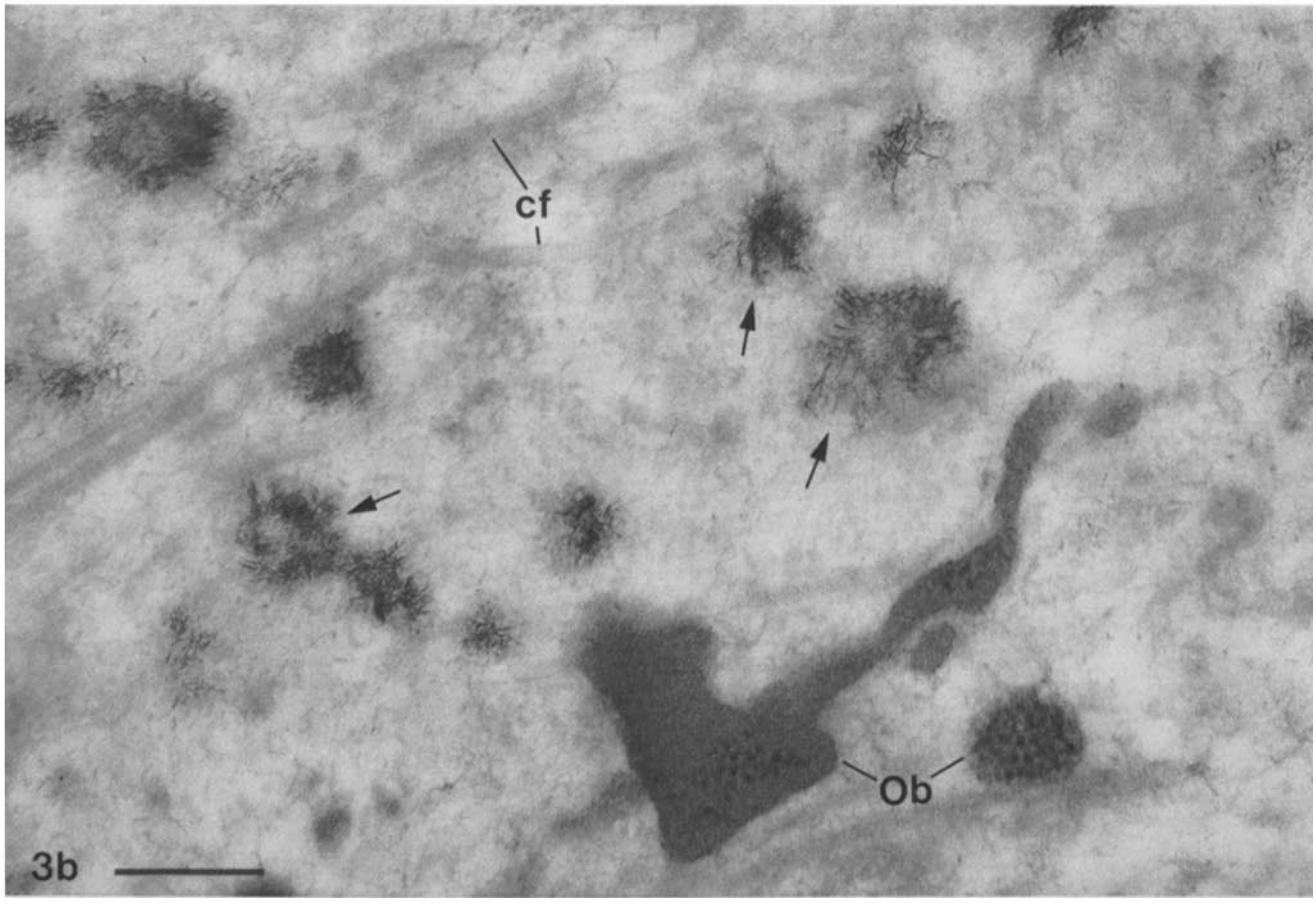
cf
Ob
3b

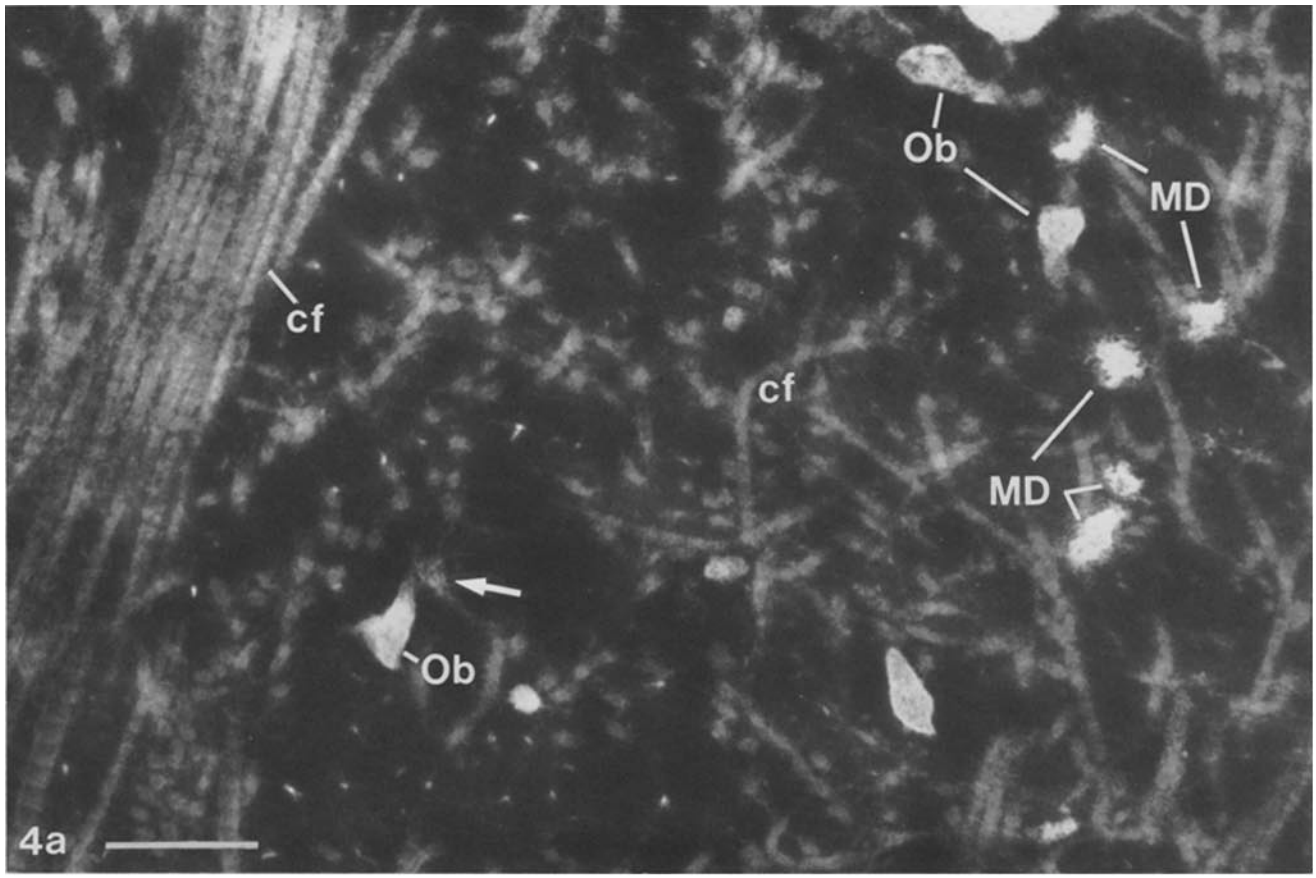
Ob
MD
cf
cf
MD
Ob
4a

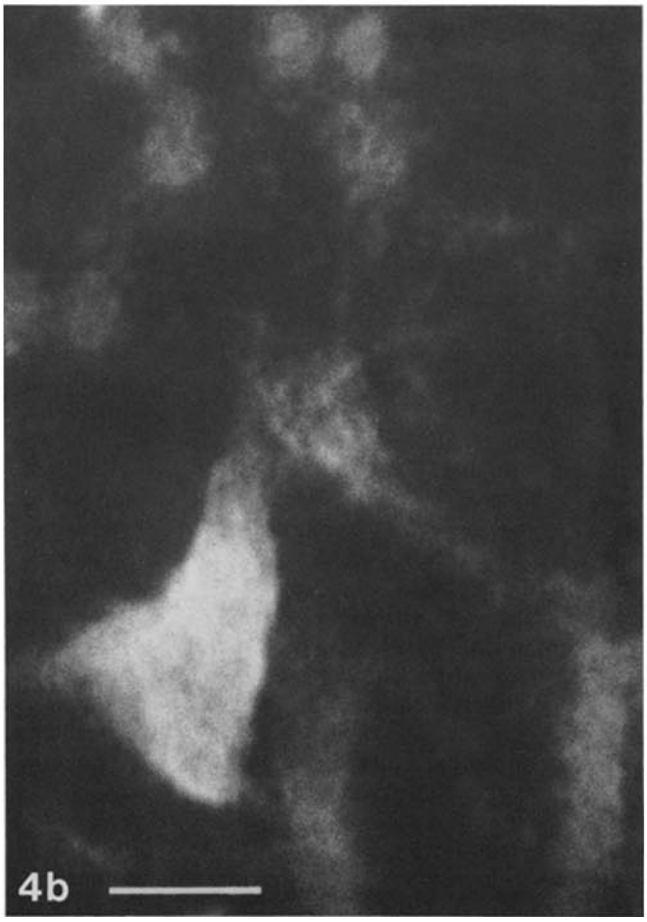
4b

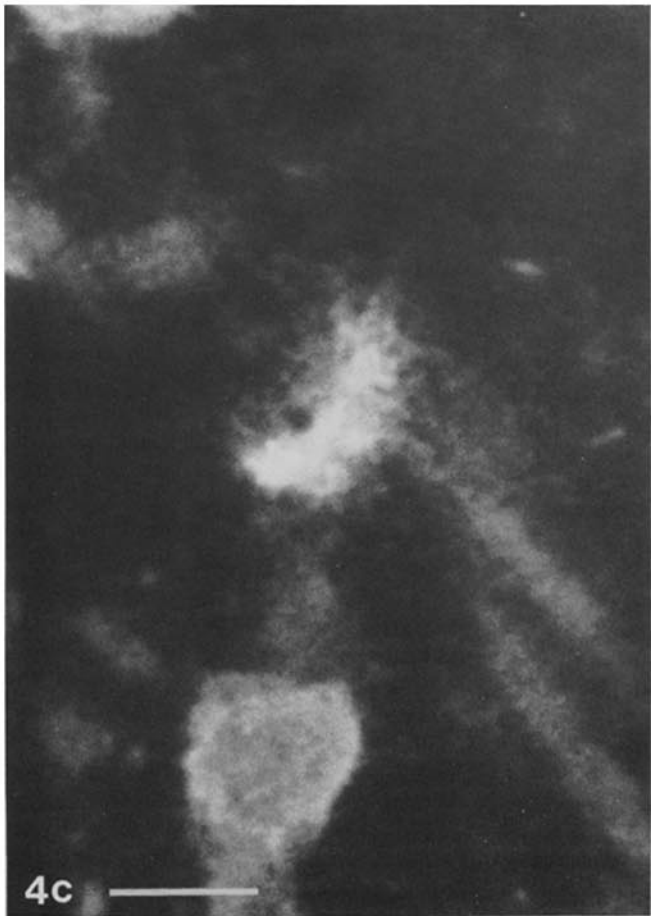
4c

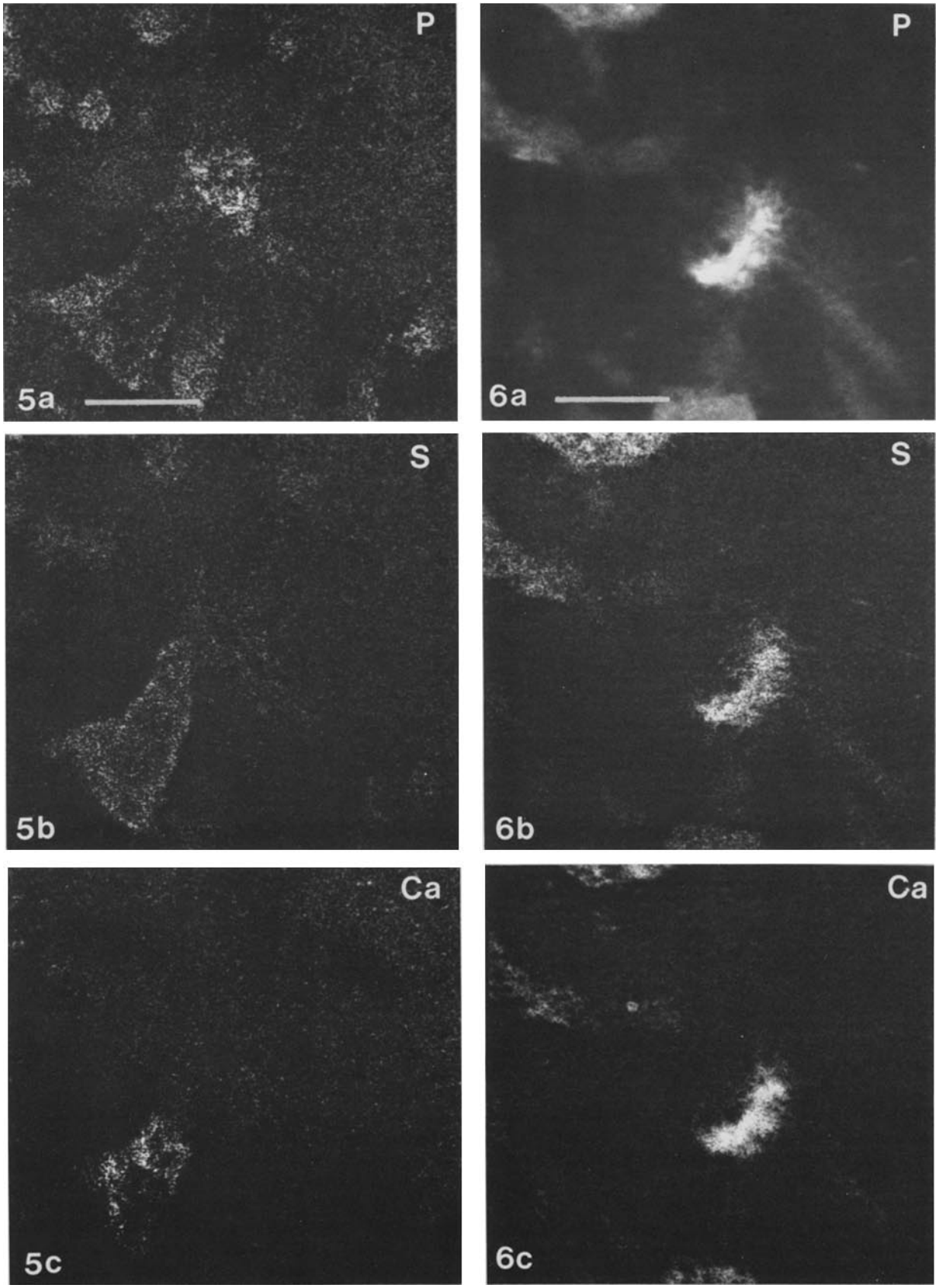

FIGURES 5 and 6 Fig. 5: Digital display images of the nucleation site in Fig. 4*b*, which shows the spatial individual elemental maps of *P*, *S*, and *Ca* in *a*, *b*, and *c*, respectively. Bars, 0.15 μm. × 140,000. Fig. 6: Elemental maps of the early mineral deposit in Fig. 4*c* displaying *P*, *S*, and *Ca* in *a*, *b*, and *c*, respectively. Bar, 0.15 μm. × 140,000.

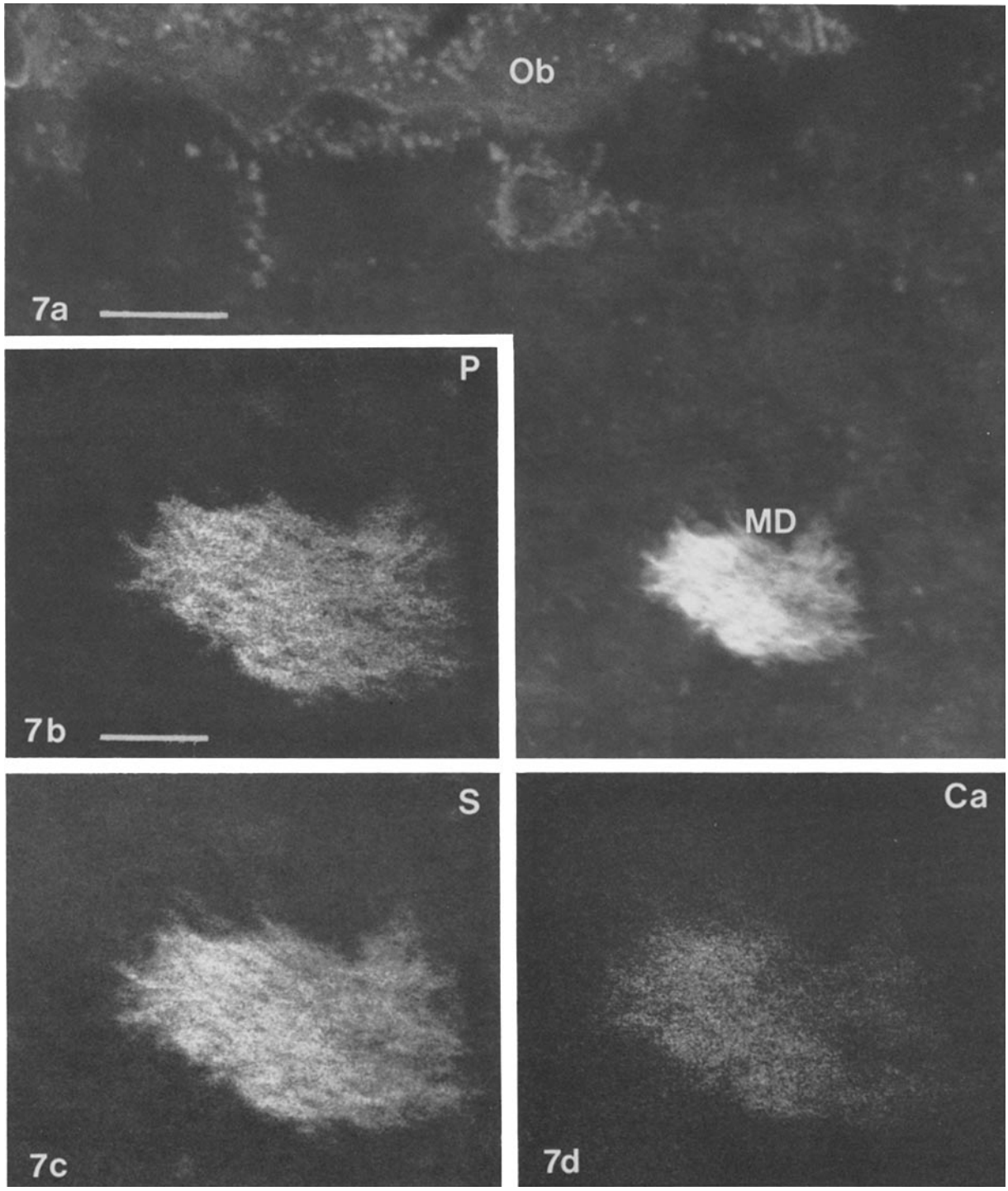

FIGURE 7 (*a*) An electron spectroscopic image at 180 eV showing a mineral deposit (*MD*) at an equivalent stage of development as those shown in Fig. 3*b*. Ob, osteoblast. (*b–d*) Elemental maps showing the distribution of P, S, and Ca, respectively. Bars, 0.2 μm (*a*); 0.1 μm (*b–d*). × 120,000 (*a*); × 170,000 (*b–d*).

plate (7). The difference between the early stages of mineralization in bone and cartilage is believed to result from distinct chemical and structural properties that characterize the unique features of the two matrices. These results suggest that at each site of nucleation and subsequent mineralization a matrix stratum containing an S-rich moiety exists and persists, serving as a scaffold on which Ca and P are locally concentrated.

The ESI visualization of S in superposition with Ca/P within mineral deposits of bone and cartilage is consistent with the appearance of crystal ghosts in formerly calcified sites after demineralization of the specimen as described by Bonucci (10, 11) after demineralization of the specimen. More recently several studies using x-ray probe microanalysis have revealed the presence of S in mineral deposits from both undemineralized and demineralized specimens (16, 21, 41). Corroborating and extending these findings is the development of specific immunofluorescent localization of cartilage-

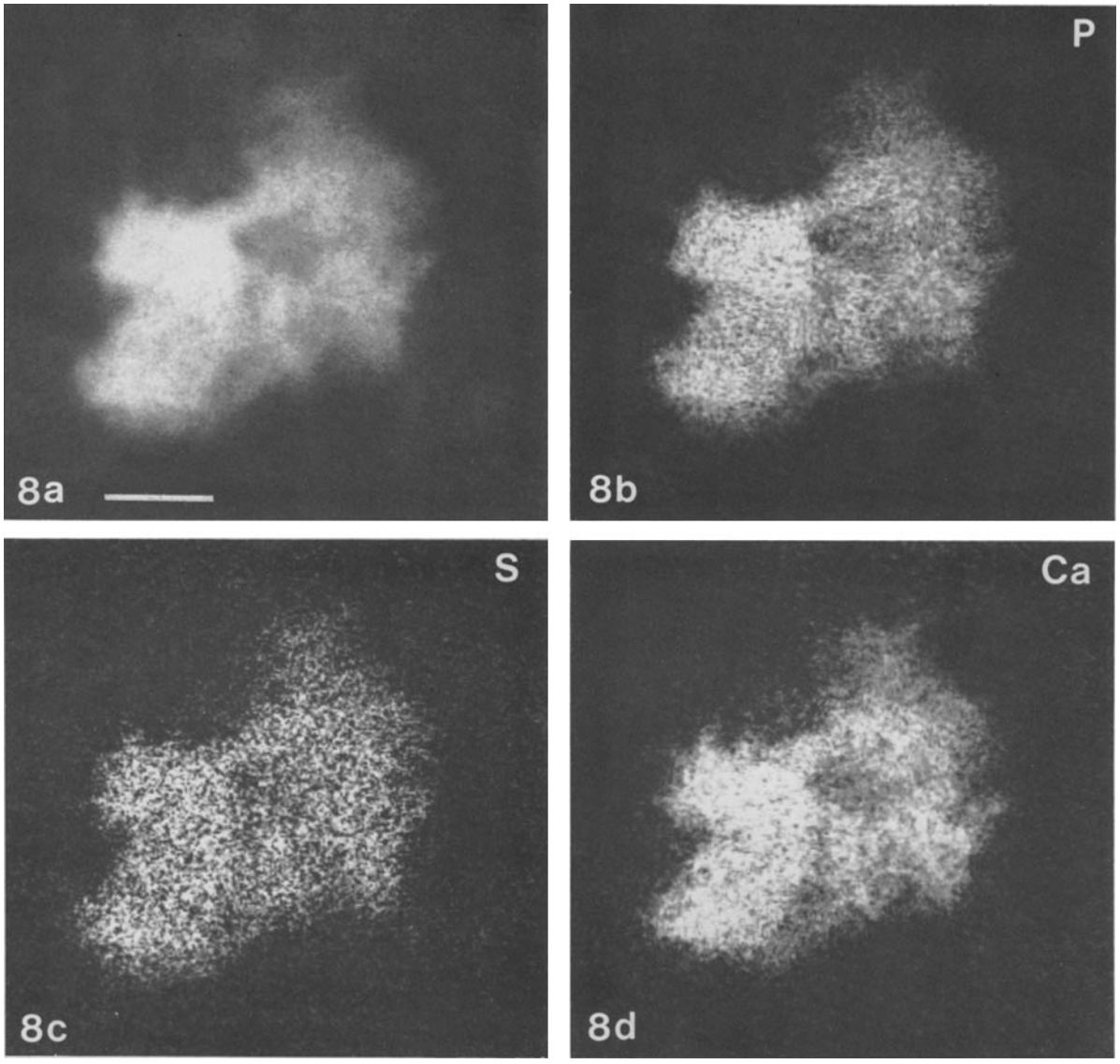

FIGURE 8 (*a*) A digitized 180 eV electron spectroscopic image of a cryofixed mineral deposit at a similar stage of advancement as that shown in Fig. 7*a*. (*b–d*) Elemental maps showing the distributions of *P*, *S*, and *Ca*, respectively. Bar, 0.05 μm. × 305,000.

link protein and proteoglycan monomers (32, 33). The localization of these antibodies in the zones of hypertrophy and the zone of provisional calcification demonstrates that proteoglycans are maintained with the advancement of mineralization and further become embedded components of mineral deposits. This persistence of proteoglycans in mineralized matrices is at variance with the formerly held opinion that proteoglycans were depleted in accordance with a physiological prerequisite to promote mineralization. However, with the development of highly specific labeling and high detection microanalytical techniques, it is apparent that some S-containing components, possibly proteoglycans, play an important and spatially intimate role in mineralization.

Bernard and Pease (8) studying intramembranous mineralization in fetal mouse calvaria illustrated calcification loci (or early mineral deposits) at equivalent stages of development as those deposits shown in the perichondrial ring in Figs. 2*c* and 4*c*. They postulated that such loci were derived from buds or vesicular components of osteoblasts. Subsequently, surveys have classified these calcification loci to be membrane-bounded matrix vesicles (5, 6), although structural evidence supporting membrane investment was not presented. Our results are not in agreement with this postulate nor with such a classification. By examining the developmental gradient of mineralization along its longitudinal axis we observed earlier stages of mineral deposit morphogenesis. At such earlier stages as that shown in Fig. 2*b* the low density of nascent mineral deposits enables the visualization of spatially associated matrix components. Thus, we have found that the nucleation sites occur in situ within the osteoid by the condensation and rearrangement of matrix components. If matrix vesicles were present at such loci they would be clearly evident, as those shown in the epiphysis (Fig. 2*a*, *inset*). In contrast, the more advanced loci reported by Bernard and Pease (8) possess occluding mineral deposits which prevents the analysis of fine structural details.

Contrary to the reported presence and involvement of matrix vesicles in intramembranous ossification (23, 29, 30, 37, 38) this study clearly shows that such membrane-bounded structures are not present as constituents of nucleation sites or mineral deposits. Potential vesicular structures at low magnification in areas such as Figs. 2 and 3 were invariably not

membrane-bounded or were clearly osteoblast extensions at higher magnifications. A careful reading of reports of matrix vesicles in bone matrices almost invariably presented images at too low a magnification for unequivocal assessment (8, 17, 29, 30, 37, 38, 42) or implicated unusual structural enhancement by phase effects in defocused bright field images (5). Moreover, the presence of matrix vesicles in these tissues cannot be easily dismissed. Our examination of murine epiphyseal cartilage in stained bright field images demonstrates the presence of the so-called matrix vesicles (Fig. 2, *inset*) not observed in perichondrial ring. We are presently attempting to characterize these cartilage structures by ESI to determine the nature of their reported limiting membrane and to examine their Ca/P sequestering role during calcification.

We conclude that the initial series of events of nucleation in the perichondrial ring involve the aggregation of S-rich matrix components that occur concomitantly with the accumulation of spatial overlaps of Ca and P. Thus, the development of the nucleation site and subsequent orderly mineralization in this context implicates a mechanism of alteration of both the chemistry and the structure of perichondrial matrix, which serves to create a microenvironment for Ca and P deposition in an intimate organic/inorganic association. Once the nucleation site has formed, the constituent S-rich matrix continues to aggregate in association with Ca/P deposition.

We thank Dr. G. Simon and Mr. E. Spitzer for providing facilities and assistance for cryofixation.

This work was supported by the National Cancer Institute of Canada, the Ontario Cancer Treatment and Research Foundation, the National Science and Engineering Research Council, and the Medical Research Council of Canada.

Received for publication 11 August 1983, and in revised form 21 November 1983.

REFERENCES

1. Adamson-Sharpe, K. M., and F. P. Ottensmeyer. 1981. Spatial resolution and detection sensitivity in microanalysis by electron energy loss selected imaging. *J. Microsc. (Oxf.).* 122:309–314.
2. Ali, S. Y. 1976. Analysis of matrix vesicles and their role in the calcification of epiphyseal cartilage. *Fed. Proc.* 35:135–142.
3. Ali, S. Y., A. Wisby, L. Evans, and J. Craig-Gray. 1977. The sequence of calcium and phosphorus accumulation by matrix vesicles. *Calcif. Tissue Res.* 22:490–493. (Suppl.)
4. Anderson, H. C. 1969. Vesicles associated with calcification in the matrix of epiphyseal cartilage. *J. Cell Biol.* 41:59–72.
5. Anderson, H. C. 1973. Calcium-accumulating vesicles in the intercellular matrix of bone. *In* Hard Tissue Growth, Repair and Mineralization. Ciba Foundation Symposium 11, Elsevier/North Holland Biomedical Press, Amsterdam.
6. Anderson, H. C. 1976. Matrix vesicle calcification. *Fed. Proc.* 35:105–108.
7. Arsenault, A. L., and F. P. Ottensmeyer. 1983. Quantitative spatial distributions of calcium, phosphorus, and sulfur in calcifying epiphysis by high resolution spectroscopic imaging. *Proc. Natl. Acad. Sci. USA.* 80:1322–1326.
8. Bernard, G. W., and D. C. Pease. 1969. An electron microscopic study of initial intramembranous osteogenesis. *Am. J. Anat.* 125:271–290.
9. Bonucci, E. 1967. Fine structure of early cartilage calcification. *J. Ultrastruct. Res.* 20:33–50.
10. Bonucci, E. 1969. Further investigation on the organic/inorganic relationships in calcifying cartilage. *Calcif. Tissue Res.* 3:38–54.
11. Bonucci, E. 1971. The locus of initial calcification in cartilage and bone. *Clin. Orthop. Relat. Res.* 78:108–139.
12. Boothroyd, B. 1964. The problem of demineralization in thin sections of fully calcified bone. *J. Cell Biol.* 20:165–173.
13. Boothroyd, B. 1968. Sources of artefact in preparation of bone for electron microscopy. *In* Electron Microscopy. D. Steve-Bocciarelli, editor. Tipografia Poliglotta Vaticana, Rome. 2:429–430.
14. Boothroyd, B. 1975. Observations on embryonic chick-bone crystals by high resolution transmission electron microscopy. *Clin. Orthop. Relat. Res.* 106:290–310.
15. Cecil, R. N. A., and H. C. Anderson. 1978. Freeze-etch studies of epiphyseal growth plate cartilage reveal matrix vesicles associated with calcification. *Proc. 9th Intl. Congr. Electron Microsc.* 2:670–671.
16. Davis, W. L., R. G. Jones, J. P. Knight, and H. K. Hagler. 1982. Cartilage calcification: an ultrastructural, histochemical, and analytical x-ray microprobe study of the zone of calcification in the normal avian epiphyseal growth plate. *J. Histochem. Cytochem.* 30:221–234.
17. Dougherty, W. J. 1978. The occurrence of amorphous mineral deposits in association with the plasma membrane of active osteoblasts in rat and mouse alveolar bone. *Metab. Bone Dis. Relat. Res.* 1:119–123.
18. Eisemann, D. R., and P. L. Glick. 1972. Ultrastructure of initial crystal formation in dentin. *J. Ultrastruct. Res.* 41:18–28.
19. Gay, C. V. 1977. The ultrastructure of the extracellular phase of bone as observed in frozen thin sections. *Calcif. Tissue Res.* 23:215–223.
20. Glimcher, M. J. 1976. Composition, structure, and organization of bone and other mineralized tissues and the mechanism of calcification. *In* Handbook of Physiology: Endocrinology. R. O. Greep and E. B. Astwood, editors. American Physiological Society, Washington, DC. 7:25–116.
21. Groot, C. G. 1982. Electron microscopical x-ray microanalysis of mineralization nodules and several other tissue components in fetal bone. *Metab. Bone Dis. Relat. Res.* 4:211–216.
22. Hunziker, E. B., W. Herrmann, and R. K. Schenk. 1982. Improved cartilage fixation by ruthenium hexammine trichloride (RHT). A prerequisite for morphometry in growth cartilage. *J. Ultrastruct. Res.* 81:1–12.
23. Kim, K. M., and S. Huang. 1971. Ultrastructural study of calcification of human aortic valve. *Lab. Invest.* 25:357–366.
24. Landis, W. J., and M. J. Glimcher. 1978. Electron diffraction and electron probe microanalysis of the mineral phase of bone tissue prepared by anhydrous techniques. *J. Ultrastruct. Res.* 63:188–223.
25. Landis, W. J., and M. J. Glimcher. 1982. Electron optical and analytical observations of rat growth plate cartilage prepared by ultracryomicrotomy: the failure to detect a mineral phase in matrix vesicles and the identification of heterodispersed particles as the initial solid phase of calcium phosphate deposited in the extracellular matrix. *J. Ultrastruct. Res.* 78:227–268.
26. Landis, W. J., B. T. Hauschka, C. A. Rogerson, and M. J. Glimcher. 1977. Electron microscopic observations of bone tissue prepared by ultracryomicrotomy. *J. Ultrastruct. Res.* 59:185–206.
27. Landis, W. J., M. C. Paine, and M. J. Glimcher. 1977. Electron microscopic observations of bone tissue prepared anhydrously in organic solvents. *J. Ultrastruct. Res.* 59:1–30.
28. Martin, J. H., and J. L. Matthews. 1969. Mitochondrial granules in chondrocytes. *Calcif. Tissue Res.* 3:184–193.
29. Martino, L. J., V. L. Yeager, and J. J. Taylor. 1979. An ultrastructural study of the role of calcification nodules in the mineralization of woven bone. *Calcif. Tissue Res.* 27:57–64.
30. Ornoy, A., I. Atkin, and J. Levy. 1980. Ultrastructural studies on the origin and structure of matrix vesicles in bone of young rats. *Acta Anat.* 106:450–461.
31. Ottensmeyer, F. P., and J. W. Andrew. 1980. High-resolution microanalysis of biological specimens by electron energy loss spectroscopy and electron spectroscopic imaging. *J. Ultrastruct. Res.* 72:336–348.
32. Ottensmeyer, F. P., A. L. Arsenault, and A. Yu. 1982. Quantitative elemental mapping in electron spectroscopic images of biological specimens. *Proc. Congr. Electron Microsc.* 1:597–598.
33. Poole, A. R., I. Pidoux, and L. Rosenberg. 1982. Role of proteoglycans in endochondral ossification: immunofluorescent localization of link protein and proteoglycan monomer in bovine fetal epiphyseal growth plate. *J. Cell Biol.* 92:249–260.
34. Poole, A. R., A. H. Reddi, and L. C. Rosenberg. 1982. Persistence of cartilage proteoglycan and link protein during matrix-induced endochondral bone development: an immunofluorescent study. *Dev. Biol.* 89:532–539.
35. Robinson, R. A., and M. L. Watson. 1952. Collagen-crystal relationships in bone as seen in the electron microscope. *Anat. Rec.* 114:383–392.
36. Sayegh, F. S., G. C. Solomon, and R. W. Davis. 1974. Ultrastructure of intracellular mineralization in the deer's antler. *Clin. Orthop. Relat. Res.* 99:267–284.
37. Schraer, H., and C. V. Gay. 1977. Matrix vesicles in newly synthesizing bone observed after ultracryotomy and ultramicroincineration. *Calcif. Tissue Res.* 23:185–188.
38. Sela, J., I. A. Bab, and A. Muhlrad. 1981. A comparative study on the occurrence and activity of extracellular matrix vesicles in young and adult rat maxillary bone. *Calcif. Tissue Res.* 33:129–134.
39. Shapiro, F., M. E. Holtrop, and M. J. Glimcher. 1977. Organization and cellular biology of the perichondrial ossification groove of Ranvier. *J. Bone Jt. Surg. Am. Vol.* 59:703–723.
40. Shepard, N., and N. Mitchell. 1976. The localization of proteoglycan by light and electron microscopy using Safranin O. A study of epiphyseal cartilage. *J. Ultrastruct. Res.* 54:451–460.
41. Shepard, N., and N. Mitchell. 1981. Acridine orange stabilization of glycosaminoglycans in beginning endochondral ossification. A comparative light and electron microscopic study. *Histochemistry.* 70:107–114.
42. Sudo, H., H.-A. Kodama, Y. Amagai, S. Yamamoto, and S. Kasai. 1983. In vitro differentiation and calcification in a new clonal osteogenic cell line derived from newborn mouse calvaria. *J. Cell Biol.* 96:191–198.
43. Takagi, M., Y. Kasahara, H. Takagi, and Y. Toda. 1979. Freeze-fracture images of matrix vesicles of epiphyseal cartilage and non-calcified tracheal cartilage. *J. Electron Microsc.* 28:165–175.
44. Thyberg, J. 1974. Electron microscopic studies on the initial phases of calcification in guinea pig epiphyseal cartilage. *J. Ultrastruct. Res.* 46:206–218.
45. Thyberg, J., S. Lohmander, and U. Friberg. 1973. Electron microscopic demonstration of proteoglycans in guinea pig epiphyseal cartilage. *J. Ultrastruct. Res.* 45:407–427.